# TORSIONAL BEHAVIOR OF THE HUMAN FEMUR

S. B. Roberts, S. K. Pathak
School of Engineering and Applied Science
University of California, Los Angeles, CA., U.S.A.

## ABSTRACT

The results of 36 dynamic torsion tests on diaphyseal segments of fresh human femora yielded average strengths of 154.7 Nm and 118.3 Nm for males and females respectively. All specimens failed with a spiral fracture surface. The results of a detailed stress analysis conducted on one femur compared favorably with measured stiffness and published ultimate shear stress values.

## INTRODUCTION

A collection of 36 fresh human femora was tested dynamically in torsion. The specimens were collected at autopsy within eight hours of death, removed intact, sealed in plastic bags and stored at 20°C until needed for testing. They were obtained from 19 females and 16 males with an average age of 58 years, height of 160 cm and weight of 65.2 kg with no bone abnormalities demonstrable at x-ray. The length of each specimen was standardized at 37 cm (lesser trochanter to flare of distal metaphysis). The proximal and distal ends were embedded in coaxial cylinders of polymethyl methacralate (8.26 cm x 6.35 cm diameter, Fig. 1). One end cylinder was securely attached to a torque transducer and the other was supported by two bearing plates and had a lever arm attached for load application. The system was designed to permit torsion to be transmitted through the end PMMA cylinders to the femoral shaft. For additional details, see (1).

In the dynamic tests, a 12 kg weight was dropped 2.9 m along a guide rod to impact the lever arm. The resulting rotation of the free end and the input torque were recorded as functions of time.

One specimen, (Femur I), was initially tested statically and subsequently dynamically tested to failure. It failed with a spiral fracture as did all of the other 35 femurs. The 3 pieces of Femur I were reassembled, glued together and sectioned normal to the longitudinal axis at 2.5 cm intervals (Fig. 1). The nine cross-sections were photographed and their 2.5X enlargements were used to define the cortical wall boundaries for the finite element analysis. Each cross-section was represented by a collection of 120 quadrilateral elements with a total of 150 nodal points (Fig. 2).

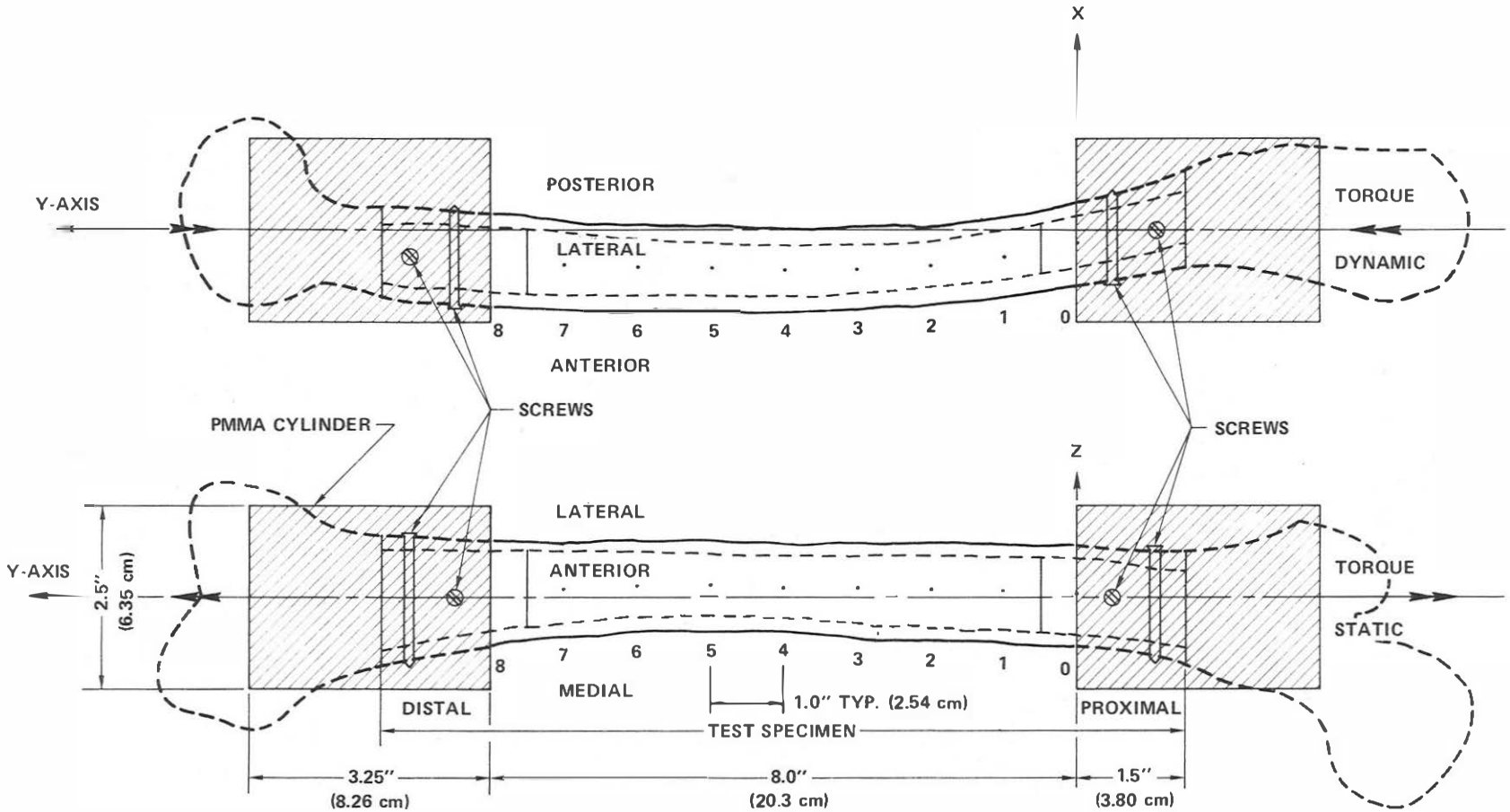


Figure 1. Femur I

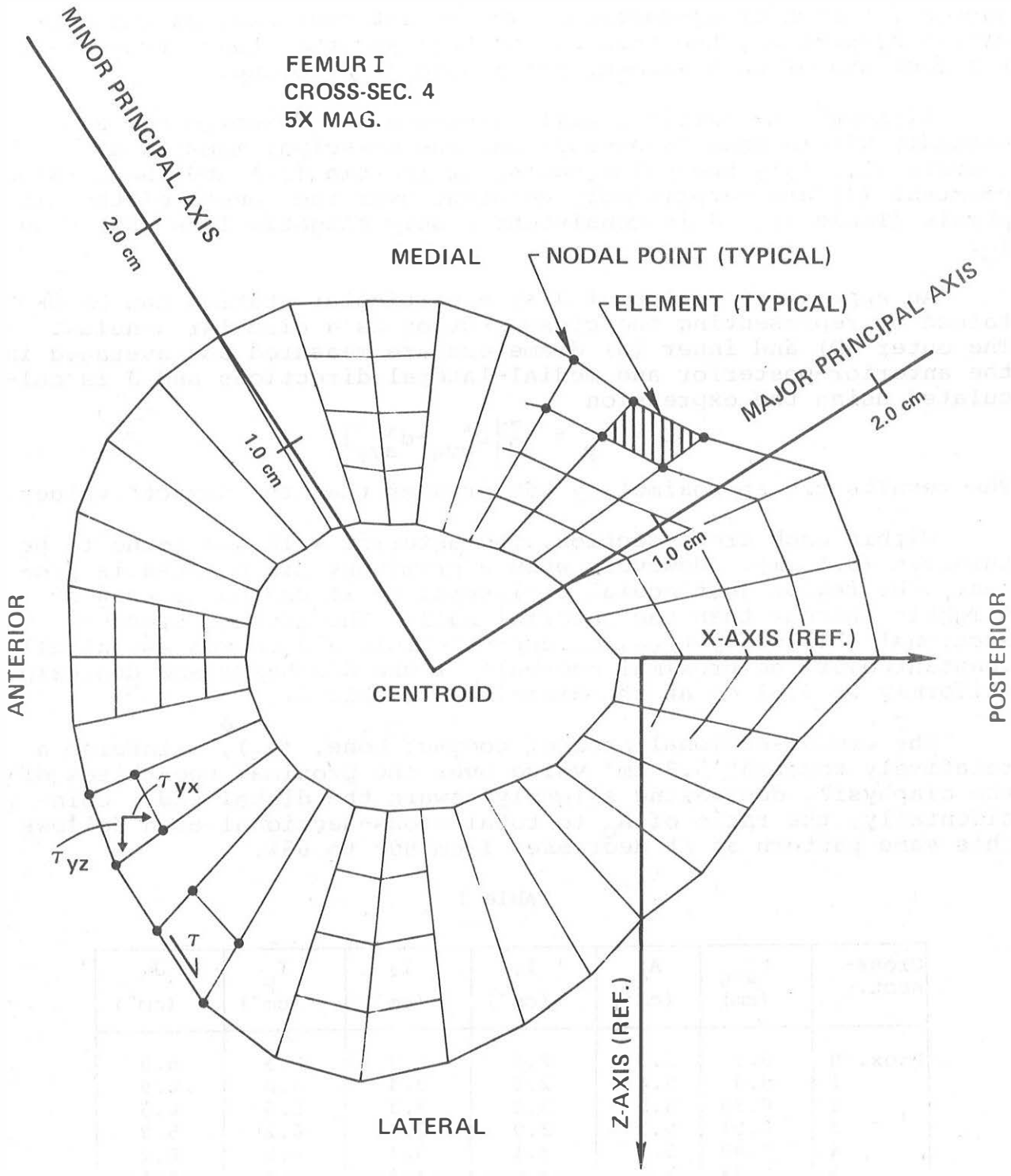


Figure 2. Typical Finite Element Representation

GEOMETRIC PROPERTIES

A finite element, St. Venant torsion analysis (2), was conducted for each cross-section. The output consisted of the geometric properties, the torsion constant and the shear stresses at the centroid of each element for a specified torque.

Although the cortical wall thickness was observed to vary markedly within each cross-section, the principal moments of inertia ($I_1$, $I_2$), the polar moment of inertia ($I_p$) and the torsion constant (J) are surprisingly constant over the length of the diaphysis (Table 1). J is consistently only slightly less (5%) than $I_p$.

An approximate value of J at a particular station can be obtained by representing the cross-section as a circular annulus. The outer (D) and inner (d) diameters are measured and averaged in the anterior-posterior and medial-lateral directions and J is calculated using the expression

$$J = I_p = \frac{\pi}{32}\left[D^4_{avg} - d^4_{avg}\right]$$

The results are approximately 15% greater than the "exact" values.

Within each cross-section, the anterior wall was found to be thinnest (0.5 cm). However, when a prominent linea aspea is present, the region just medial or lateral to it can be as thin or slightly thinner than the anterior wall. The average cross-sectional thickness, $t_{avg}$, of approximately 0.9 cm was essentially constant over the proximal one-half of the diaphysis and decreased uniformly to 0.51 cm at the distal end (Table 1).

The cross-sectional area of compact bone, ($A_c$), maintains a relatively constant 5.3 $cm^2$ value over the proximal two-thirds of the diaphysis, decreasing slightly toward the distal end. Coincidentally, the ratio of $A_c$ to total cross-sectional area follows this same pattern as it decreases from 80% to 65%.

Table 1

| Cross-sect. | $t_{avg}$ (cm) | $A_c$ ($cm^2$) | $I_1$ ($cm^4$) | $I_2$ ($cm^4$) | $I_p$ ($cm^4$) | J ($cm^4$) |
|---|---|---|---|---|---|---|
| Prox. 0 | 0.9 | 5.3 | 2.6 | 3.7 | 6.3 | 6.0 |
| 1 | 0.9 | 5.4 | 2.8 | 3.4 | 6.2 | 6.0 |
| 2 | 0.95 | 5.5 | 3.2 | 3.3 | 6.5 | 6.3 |
| 3 | 0.91 | 5.3 | 2.9 | 3.3 | 6.2 | 5.9 |
| 4 | 0.88 | 5.3 | 3.1 | 3.4 | 6.5 | 6.2 |
| 5 | 0.83 | 5.1 | 3.0 | 3.4 | 6.4 | 6.1 |
| 6 | 0.7 | 4.8 | 2.8 | 3.3 | 6.1 | 5.9 |
| 7 | 0.56 | 4.6 | 3.2 | 3.4 | 6.6 | 6.5 |
| Dist. 8 | 0.51 | 4.5 | 3.2 | 3.8 | 7.0 | 6.9 |

## STRESS ANALYSIS

The shear stress stresses ($\tau_{yz}$, $\tau_{yx}$), (Fig. 2), and the rate of twist $\theta$, within each cross-section were determined from the finite element solution to the St. Venant torsion problem for an isotropic (or transversely isotropic) material. Specifically, a warping function $\phi(x,z)$ which satisfies Laplaces equation $\nabla^2\phi=0$ in the plane and the boundary conditions was calculated numerically (2) and the quantities of interest were obtained by direct operations on $\phi$, namely:

$$\tau_{yz}=G\theta\left(x+\frac{\partial\phi}{\partial z}\right) \qquad G = \text{shear modulus}$$

$$\tau_{yx}=G\theta\left(-z+\frac{\partial\phi}{\partial x}\right) \qquad \tau = \sqrt{\tau_{yz}^2+\tau_{yx}^2}$$

$$J=\int_A\left[x^2+z^2+x\frac{\partial\phi}{\partial z}-z\frac{\partial\phi}{\partial x}\right]dA$$

The resultant shear stress ($\tau$) was also calculated at the element mid-points and extrapolated to the external cortical wall. The value of $\tau_{max}$ was obtained for each cross-section and plotted in Fig. 3. It was found to occur at one of three locations; anteriorly, posteromedially or posterolaterally. These are the regions at which (a) the cortical wall is thinnest and/or (b) a prominent linea aspea gives rise to a local reentrant corner posteromedially.

For comparison purposes, each cross-section was also modeled as a circular annulus with the same $A_c$ and $I_p$. The maximum shear stresses were calculated and as can be observed from Fig. 3, this approximation consistently underestimates $\tau_{max}$ by as much as 50%.

The torsional stiffness for the entire 20.3 cm shaft was calculated on the basis of a static shear modulus, $G=3.5\times10^6 KN/m^2$ and found to be 16.4 Nm/deg. This value is plotted in Fig. 4. According to McElhaney (3), the ratio of the modulus of elasticity at a strain rate of 1 $sec^{-1}$ to that in a "static" test is approximately 1.4. If we assume this same ratio applies to the shear modulus, then we would anticipate a dynamic torsional stiffness of 23 Nm/deg (Fig. 4).

## EXPERIMENTAL RESULTS

The results of the 36 dynamic tests are displayed in Table 2. The average failure torque for all tests compares favorably with the value of 137 Nm reported by Yamada (4). However, the total angular twist of 1.5° reported in (4) is considerably below the 13.3° obtained in this series.

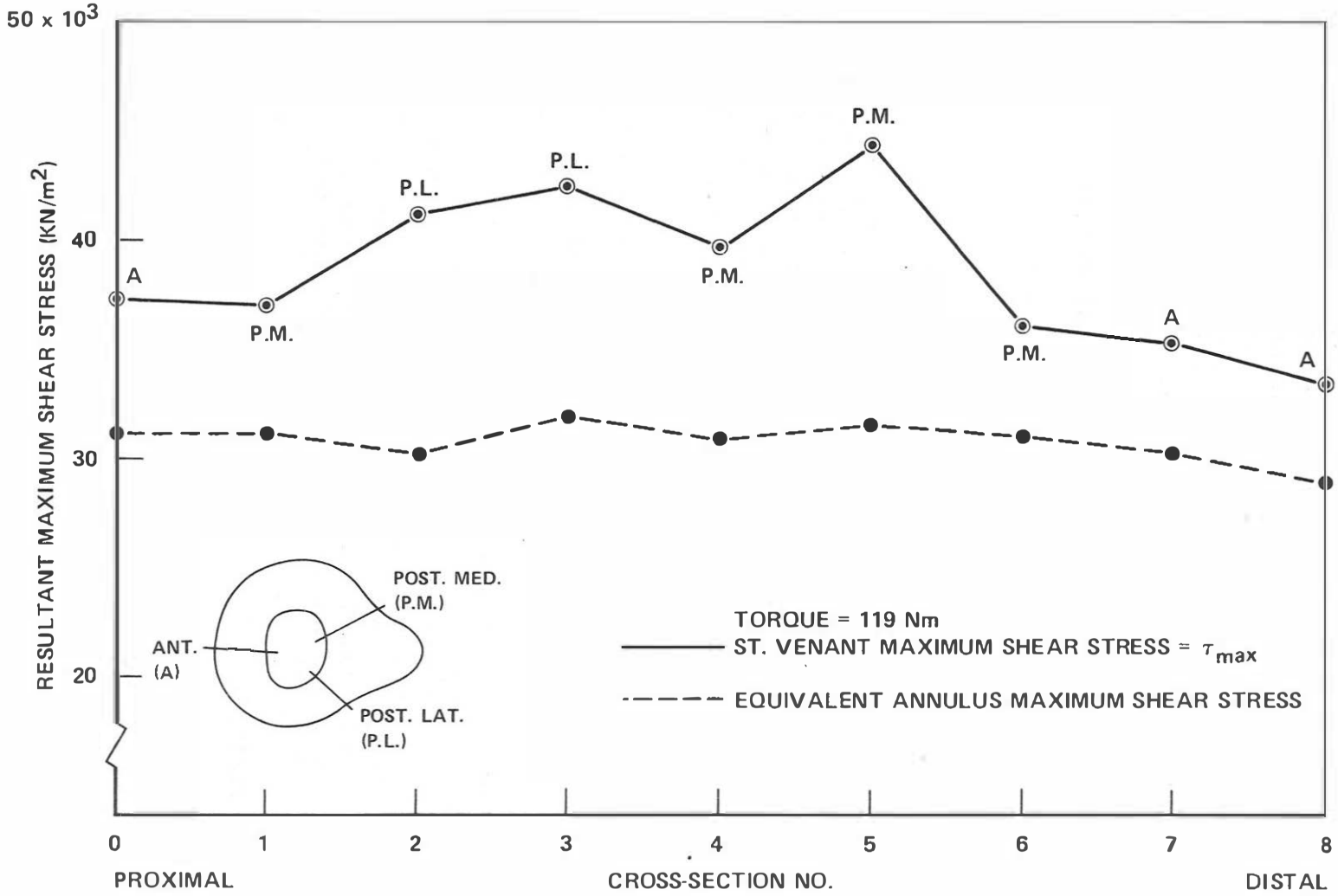


Figure 3. Calculated Maximum Shear Stresses

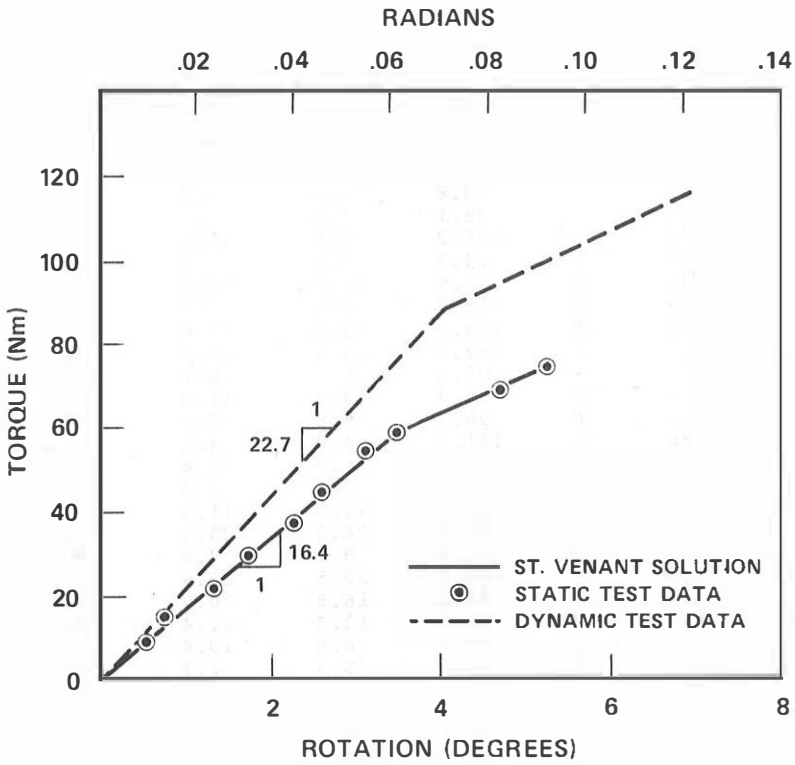


Figure 4. Torque vs. Rotation

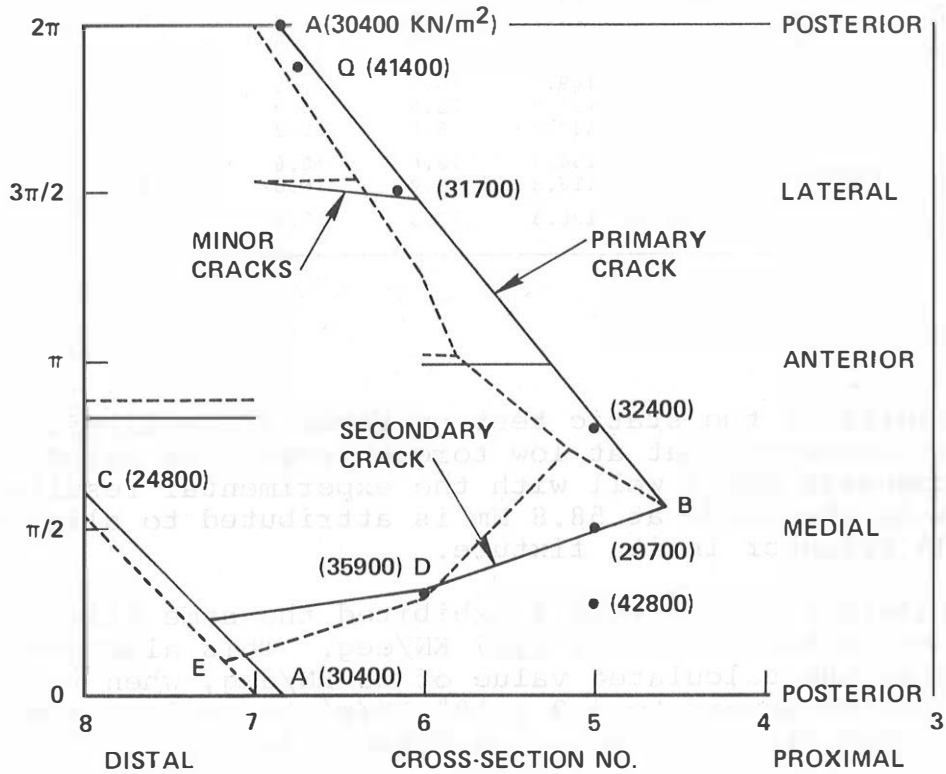


Figure 5. Femur I, Developed Crack Surface

Table 2

| Specimen No. | Age (Yrs.) | Sex | Failure Torque (Nm) | Rotation to Failure (Degrees) | Failure Energy (Nm) | Failure Time (Millisec.) |
|---|---|---|---|---|---|---|
| 1 | 76 | F | 90.8 | 11.0 | 8.7 | 4.8 |
| 2 | 64 | F | 85.1 | 7.5 | 5.5 | 4.2 |
| 3 | 69 | M | 155.2 | 9.1 | 12.3 | 5.7 |
| 4 | 64 | F | 84.3 | 7.6 | 5.6 | 4.0 |
| 5 | 46 | F | 105.9 | 10.0 | 9.2 | 4.5 |
| 6 | 49 | M | 110.7 | 8.0 | 7.7 | 4.8 |
| 7 | 84 | M | 212.8 | 24.0 | 44.6 | - |
| 8 | 55 | F | 141.9 | 28.0 | 12.3 | 6.5 |
| 9 | 65 | M | 96.9 | 6.0 | 5.0 | 3.0 |
| 10 | 73 | F | 99.3 | 13.8 | 11.9 | 5.2 |
| 11 | 50 | F | 98.7 | 8.8 | 7.6 | 5.0 |
| 12 | 86 | M | 131.3 | 4.0 | 4.5 | 4.3 |
| 13 | 76 | F | 135.0 | 19.0 | 22.4 | 11.4 |
| 14 | 70 | M | 98.7 | 6.3 | 5.4 | 3.5 |
| 15 | 54 | F | 120.3 | 11.0 | 11.5 | 3.5 |
| 16 | 33 | M | 197.6 | 14.0 | 23.7 | 9.5 |
| 17 | 72 | M | 118.0 | 9.2 | 9.5 | 9.3 |
| 18 | 52 | F | 204.6 | 20.5 | 36.6 | 12.0 |
| 19 | 56 | F | 143.6 | 16.8 | 20.9 | 9.0 |
| 20 | 61 | M | 185.5 | 13.3 | 21.4 | 8.3 |
| 21 | 33 | M | 138.2 | 8.6 | 10.4 | 4.0 |
| 22 | 48 | F | 46.8 | 5.5 | 2.2 | 4.3 |
| 23 | 47 | F | 161.6 | 17.5 | 24.7 | 10.0 |
| 24 | 58 | F | 56.9 | 7.8 | 3.9 | 2.5 |
| 25 | 44 | M | 190.7 | 9.5 | 15.7 | 4.5 |
| 26 | 60 | F | 158.9 | 32.0 | 44.3 | 20.7 |
| 27 | 68 | M | 100.6 | 7.4 | 6.4 | 3.5 |
| 28 | 62 | F | 139.0 | 15.6 | 18.9 | 5.5 |
| 29 | 54 | F | 69.8 | 9.2 | 5.6 | 4.0 |
| 30 | 24 | M | 201.1 | 16.0 | 28.0 | 10.5 |
| 31 | 75 | F | 130.5 | 10.0 | 31.3 | 6.5 |
| 32 | 68 | M | 227.0 | 27.5 | 54.4 | - |
| 33 | 49 | F | 174.2 | 14.5 | 22.0 | 8.0 |
| 34 | 42 | M | 169.7 | 13.9 | 20.6 | 6.5 |
| 35 | 61 | M | 141.9 | 25.5 | 30.9 | - |
| I | - | - | 137.2 | 8.0 | 10.3 | 6.2 |
| Averages: | | M | 154.7 | 12.6 | 18.8 | 5.95 |
| | | F | 118.3 | 14.0 | 16.0 | 6.5 |
| | | Overall | 136.5 | 13.3 | 17.4 | 6.2 |

The results of the static test on Femur I are displayed in Fig. 4. One observes that at low torque levels the calculated stiffness compares quite well with the experimental results. The sharp break in the curve at 58.8 Nm is attributed to slipping of the end PMMA cylinder in its fixture.

The dynamic test on Femur I exhibited the same bilinear character with an initial slope of 22.7 KN/deg. This also compares favorably with the calculated value of 23 KN/deg, when the shear modulus is scaled upward to $4.9 \times 10^6$ KN/m$^2$ to reflect the considerably higher strain rate in the dynamic tests.

Femur I failed with a classic helical brittle fracture

pattern at 137.2 Nm. The developed fracture surface is shown in Fig. 5. The primary crack runs along BA and AC at an angle of approximately 50° with respect to the longitudinal axis. A secondary crack connects points B and E forming the completed fracture surface.

The calculated values of $\tau_{max}$ at those points where the fracture surface intersects the cross-sections are also shown in Fig. 5. A close examination of the fracture surface revealed a local thinning of the cortical wall 0.5 cm from section 7 at point Q. The observed 35% reduction in wall thickness resulted in a value of $\tau_{max} \simeq 41400$ KN/m$^2$ at point Q, which was within 3% of the calculated maximum value at cross-section 5. This suggests that the crack could have readily initiated at either of these two locations with local conditions governing its origin.

The calculated value of $\tau_{max}$ at failure is consistent with the average value of 44850 KN/m$^2$ reported by Yamada (4) but considerably less than Reilly's (5), 67620 KN/m$^2$.

## CONCLUSIONS

From the series of 36 dynamic torsional tests on fresh human femoral shafts, we can conclude that:

(a) the average torsional load carry capacity is 154.7 Nm for males and 118.3 Nm for females at average loading rates of 26 KNm/sec and 18 KNm/sec respectively,

(b) the average rate of twist at failure for all specimens is 0.36 degrees/cm,

(c) the fracture surfaces are invariably of a spiral configuration and require an average energy input of 17.4 Nm to precipitate them,

(d) most femurs exhibit linear torque-rotation curves up to the point of fracture.

A static test and a detailed stress analysis carried out on one femur demonstrated that:

(a) the torque twist relationship is approximately linear at low stress levels,

(b) linear torsion theory can adequately estimate torsional stiffness, internal shear stresses, and torsional strength, provided that local perturbations in the cross-sectional geometry can be faithfully represented.

REFERENCES

(1) Mensch, J.S., K.L. Markloff, S.B. Roberts and G.M. Finerman, "Experimental Stabilization of Segmental Defects in the Human Femur", J. of Bone and Joint Surgery, Vol. 58 (A), No. 2, pp. 185-190, March 1976.

(2) Mason, W.E., L.R. Herrmann, "Elastic Analysis of Irregular Shaped Prismatic Beams by the Method of Finite Elements", Dept. of Civil Engineering, University of California, Davis, Technical Report No. 67, 1967.

(3) McElhaney, J., "Dynamic Response of Bone and Muscle Tissue", J. of Applied Physiology, 21 (4), pp. 1231-1236, 1966.

(4) Yamada, H., Strength of Biological Materials, Williams and Wilkins, Baltimore, Md., 1970.

(5) Reilly, D.T., and A.H. Burstein, "The Elastic and Ultimate Properties of Compact Bone Tissue", J. of Biomechanics, 8(6), pp. 393-405, December 1975.